Full Paper

Israel Journal of Chemistry

DOI: 10.1002/ijch.201700134

CO_2 Conversion Enhancement in a Periodically Operated Sabatier Reactor: Nonlinear Frequency Response Analysis and Simulation-based Study

Robert Currie,[a] Daliborka Nikolic,[b] Menka Petkovska,[c] and David S.A. Simakov*[a]

Abstract: Conversion of CO_2 into synthetic CH_4 via thermocatalytic hydrogenation (the Sabatier reaction), has recently gained increasing interest as a possible route for CO_2 utilization and energy storage pathway. Herein, we analyze the possibility of increasing the CO_2 conversion through periodic operation of the reactor. The analysis is performed by using the Nonlinear Frequency Response (NFR) method, a recently developed analytical technique, suitable for fast evaluation of periodic reactor operations. The NFR analysis predicts a significant conversion gain (up to 50%) for certain frequencies of the feed flow rate modulation. This prediction is validated by numerical simulations with a reaction rate expression obtained by CO_2 conversion experiments using a Ni/Al_2O_3 catalysts. Both the NFR analysis and numerical simulations predict that it is possible to obtain 70% CO_2 conversion at 500 K, 5 bar, and average space velocity of 7600 h^{-1} by a periodic modulation of the feed flow rate, as compared to the corresponding steady state CO_2 conversion of 43%.

Keywords: Sabatier reactor · periodic operation · nonlinear frequency response

1. Introduction

The increasing levels of global CO_2 emissions has prompted research in utilizing CO_2 as a feedstock for generating synthetic fuels and chemicals.[1] The current industrial usage of CO_2 is limited to processes such as synthesis of urea, salicylic acid and polycarbonates. Conversion of CO_2 into synthetic CH_4 via thermocatalytic hydrogenation (the Sabatier reaction, equation 3), has recently gained increasing interest as a technologically advantageous route for CO_2 utilization.[2] The Sabatier reaction is accompanied by the CO methanation and reverse water gas shift (RWGS) reactions, equations 1, 2. The extent of CO formation is mainly a function of temperature. As the Sabatier reaction is highly exothermic and results in a decrease in total number of moles, lower temperatures and higher pressures are favorable for CH_4 formation. Due to kinetic limitations, the CO_2 conversion drops sharply for $T < 600$ K, with virtually no CH_4 formation below 450 K.[3]

$$CO + 3H_2 \rightleftarrows CH_4 + H_2O \qquad \Delta H^\circ_{298} = -206.1\,kJ/mol \qquad (1)$$

$$CO_2 + H_2 \rightleftarrows CO + H_2O \qquad \Delta H^\circ_{298} = 41.2\,kJ/mol \qquad (2)$$

$$CO_2 + 4H_2 \rightleftarrows CH_4 + 2H_2O \qquad \Delta H^\circ_{298} = -164.9\,kJ/mol \qquad (3)$$

Microchannel, monolith, three-phase slurry, and fluidized bed reactors were suggested as design solutions for carrying out CO_2 methanation, as well as the packed bed configuration.[2b,c] Thermal management remains one of the main problems, as the overall process is highly exothermic requiring efficient heat removal to drive the CH_4 formation and, importantly, to prevent catalyst deactivation.[2b] While operation at the lower temperature range of 500–600 K is beneficial from the point of view of reducing the catalyst deactivation rate, CO_2 conversion is relatively low in this temperature range.[3] It is of crucial importance therefore to increase the CO_2 conversion at low temperatures. One way to improve the reactor performance is to operate it in a periodic regime,[4] which can be analyzed by the Nonlinear Frequency Response (NFR) technique.

The NFR method is a theoretical, simple and reliable general method for analysis of forced periodically operated chemical reactors.[4] It enables both qualitative and quantitative evaluation of the possibility of process improvements through periodic operations. Frequency response is defined as the periodic steady-state obtained when an input into a system is modulated in a sinusoidal or co-sinusoidal way. For a stable linear system, the frequency response is obtained as a periodic function of the same shape and frequency as the input modulation. For a *weakly nonlinear system* the frequency response is a complex periodic function[5] composed of the

[a] R. Currie, D. S. Simakov
Department of Chemical Engineering, University of Waterloo, Waterloo, ON, Canada
Tel.: +1 519 8884567
E-mail: dsimakov@uwaterloo.ca
[b] D. Nikolic
Institute of Chemistry, Technology and Metallurgy, University of Belgrade, Serbia
[c] M. Petkovska
Department of Chemical Engineering, Faculty of Technology and Metallurgy, University of Belgrade, Serbia

basic harmonic, higher harmonics, and a non-periodic (the so-called DC) component:[5b]

$$x(t) = x_s + A\ \cos(\omega t)\ \Rightarrow$$
$$y = y_s + y_{DC} + B_I \cos(\omega t + \phi_I) + B_{II} \cos(2\omega t + \phi_{II}) + B_{III} \cos(3\omega t + \phi_{III}) + \cdots \quad (4)$$

In equation 4, y_s is the steady-state value of the output corresponding to a constant input x_s. As a direct consequence of equation 4, the mean (time-averaged) value of the output y^m is different from the corresponding steady-state value y_s, with this difference being equal to the DC component:

$$\Delta = y^m - y_s = y_{DC} \quad (5)$$

If the output of interest is a product molar flow-rate at the outlet from a chemical reactor, y_{DC} becomes a measure of the possible improvement of the reactor performance owing to periodic modulation of the input x and the improvement is possible only for $y_{DC} > 0$. On the other hand, if y is the reactant molar flow-rate at the reactor outlet, the improvement is possible only for $y_{DC} < 0$.

A convenient approach for mathematical analysis of weakly nonlinear systems is the so-called concept of higher order frequency response functions (FRFs).[5b] This concept is based on replacing a nonlinear model of a weakly nonlinear system by a set of linear frequency response functions (FRFs) of different orders:

$$\mathbf{G} \equiv G_1(\omega),\ G_2(\omega_1, \omega_2),\ G_3(\omega_1, \omega_2, \omega_3), \cdots \quad (6)$$

These FRFs are directly related to different harmonics and the DC component of the output defined in equation 4.[5b] For the DC component this relation is described by the following equation:

$$y_{DC} = 2(A/2)^2 G_2(\omega, -\omega) + 6(A/2)^4 G_4(\omega, \omega, -\omega, -\omega) + \cdots \quad (7)$$

For weakly nonlinear systems the contribution of the terms proportional to the higher order FRFs decreases with the increase of their order,[5b] thus the following approximation can be used:

$$y_{DC} \approx 2(A/2)^2 G_2(\omega, -\omega) \quad (8)$$

Equation 8 is the basis of the nonlinear frequency response (NFR) method for fast evaluation of periodic operations. The function $G_2(\omega, -\omega)$ is the so-called asymmetrical second order FRF (ASO FRF), and it can be derived starting from the nonlinear model of the system.[4] Based on the sign of this function, it is possible to answer whether periodic modulation of the chosen input would result in a production rate improvement.

During the last decade the NFR method was applied for analysis of periodic operations of chemical reactors.[4,6] The method was extended to periodic operations with simultaneous modulation of two inputs,[6b,e,f,h] and to periodic modulations of wave-shapes different from sinusoidal.[6g] Isothermal,[6a,b] general nonisothermal,[6c–e,h] and adiabatic reactors[6f] were analyzed. Although the NFR method was mostly applied to the analysis of a continuous stirred tank reactor (CSTR) with a simple homogeneous reaction, simple isothermal reactions in a plug flow reactor (PFR),[6a] and in a tubular reactor with axial dispersion[6a] were also analyzed. The validity of the analytical predictions obtained by the NFR method was proven through the comparison with the results obtained by numerical simulations.

2. Results and Discussion

We start with a formulation of a simple flow reactor model. The model is then analyzed analytically by the NFR method to derive the asymmetrical second order frequency response function (ASO FRF). For the actual calculation of the time-averaged value of the chosen objective function of interest (CO_2 conversion) and its improvement, kinetic parameters (activation energies and frequency factors of reaction rates) are required. These parameters were determined experimentally, using a (commercial) Ni/Al_2O_3 catalyst as a model system. The results of the analytical predictions in frequency domain using experimentally obtained kinetic parameters are discussed and compared to numerical simulations of the originally derived flow reactor model. Eventually, selected results are presented in time domain to determine the applicability of the analytical prediction for periodic operation of a lab-scale Sabatier reactor.

2.1 Model Derivation

A simple isothermal flow reactor model (non-distributed) was derived in a dimensionless form to describe the effects of temperature and space velocity on the CO_2 conversion and selectivity to CH_4 formation (c_i is molar concentration, c_{tf} is feed molar density, L is catalytic bed length, v_g is gas velocity, W_c is catalyst bed weight, and F_{tf} is the total molar feed flow rate):

$$\frac{du_i}{d\tau} = u_{if} - u_i + Da(\alpha_{i1}\kappa_1 f_1 + \alpha_{i2}\kappa_2 f_2 + \alpha_{i3} f_3)$$
$$u_i = \frac{c_i}{c_{tf}} \qquad \tau = \frac{t}{L/v_g} \qquad Da = \frac{W_c k_3}{F_{tf}\sqrt{P}}$$
$$\kappa_1 = \frac{k_1}{k_3} = \frac{A_1}{A_3}\exp\left(\frac{E_{a3} - E_{a1}}{R_g T}\right) \tag{9}$$
$$\kappa_2 = \frac{P^{1.5}k_2}{k_3} = \frac{P^{1.5}A_2}{A_3}\exp\left(\frac{E_{a3} - E_{a2}}{R_g T}\right)$$

In the above equation, u_i is a dimensionless concentration of species i; i stands for CO_2, H_2, CH_4, CO, and H_2O, i.e., all species participating, equations (1–3). Da is the Damköhler number (note that F_{tf} can be constant, as well as time-dependent in case of periodic operation), κ_1, κ_2 are dimensionless rate constants, and f_1-f_3 represent dimensionless reaction rates with corresponding stoichiometric coefficients α_{i1}–α_{i3}:

$$f_1 = \frac{1}{\sqrt{\delta}}\frac{u_{CH_4}u_{H_2O}}{u_{H_2}^{2.5}} - \delta^{1.5}\frac{u_{H_2}^{0.5}u_{CO}}{k_{1,eq}} \tag{10a}$$

$$f_2 = \delta\left(\frac{u_{CO}u_{H_2O}}{u_{H_2}} - \frac{u_{CO_2}}{k_{2,eq}}\right) \tag{10b}$$

$$f_3 = \frac{1}{\sqrt{\delta}}\frac{u_{CH_4}u_{H_2O}^2}{u_{H_2}^{3.5}} - \delta^{1.5}\frac{u_{H_2}^{0.5}u_{CO_2}}{k_{3,eq}} \tag{10c}$$
$$k_{j,eq} = \frac{K_{j,eq}}{P^2} j = 1,3; \qquad k_{2,eq} = K_{2,eq}$$

In the dimensionless reaction rates, $k_{j,eq}$ are dimensionless equilibrium constants and δ is the ratio of the inlet and outlet total molar density (for simplicity, it is assumed that $\delta = 1$ that is $c_{tf} = c_t$, which only holds for diluted systems). The original dimensional reaction terms are given in Appendix A. Although assuming isothermal operation and not accounting for spatial distribution, equation 9 describes well a lab-scale flow reactor typically used for catalytic performance evaluation,[7] which can be eventually used for a proof-of-concept experiment. The model does account for temperature and space velocity (feed flow rate) dependence.

For applying the NFR method it is convenient to define all variables as relative deviations from their values at steady state operation. By introducing these new variables, equation 9 is redefined as follows ($u_{i,ss}$, $F_{tf,ss}$ and f_j^{ss} stand for steady state values, see Appendix B for details):

$$(1+q)\frac{dC_i}{d\tau} = (1+q)\frac{u_{if,s}}{u_{i,s}} - (1+q)(1+C_i) +$$
$$+\frac{Da_{ss}}{u_{i,ss}}\left[\alpha_{i1}\kappa_1\left(f_1^{ss} + f_1^{d}\right) + \alpha_{i2}\kappa_2\left(f_2^{ss} + f_2^{d}\right) + \alpha_{i3}\left(f_3^{ss} + f_3^{d}\right)\right]$$
$$C_i = \frac{u_i(\tau) - u_{i,ss}}{u_{i,ss}} \qquad q = \frac{F_{tf}(\tau) - F_{tf,ss}}{F_{tf,ss}} \qquad Da_{ss} = \frac{W_c k_3}{F_{tf,ss}\sqrt{P}} \tag{11}$$

Note that the Damköhler number is now defined with a constant total feed flow rate. For steady state operation, equation 11 takes the following form:

$$0 = \frac{u_{if,ss}}{u_{i,ss}} - 1 + \frac{Da_{ss}}{u_{i,ss}}\left[\alpha_{i1}\kappa_1 f_1^{ss} + \alpha_{i2}\kappa_2 f_2^{ss} + \alpha_{i3} f_3^{ss}\right] \tag{11a}$$

After incorporation of equation 11a into equation 11 and expansion all nonlinear terms in Taylor series (see Appendix A), the following equation is obtained ($i = CO_2$, H_2, CH_4, CO, H_2O):

$$(1+q)\frac{dC_i}{d\tau} = \left(\frac{u_{if,s}}{u_{i,s}} - 1\right)q - (1+q)(1+C_i) + \psi \tag{12}$$

$$\Psi = (-\Lambda_{i,1}C_{CH_4} - \Lambda_{i,2}C_{H_2O} - \Lambda_{i,3}C_{CO} - \Lambda_{i,4}C_{CO_2} - \Lambda_{i,5}C_{H_2} +$$
$$W_{i,1}C_{H_2O}^2 + W_{i,2}C_{H_2}^2 + W_{i,3}C_{CH_4}C_{H_2O} + W_{i,4}C_{CH_4}C_{H_2} +$$
$$W_{i,5}C_{H_2O}C_{CO} + W_{i,6}C_{H_2O}C_{H_2} + W_{i,7}C_{H_2}C_{CO} + W_{i,8}C_{H_2}C_{CO_2} +)$$

The auxiliary parameters $\Lambda_{i,1}$ to $\Lambda_{i,5}$ and $W_{i,1}$ to $W_{i,8}$ are defined in Appendix B.

2.2 Nonlinear Frequency Response (NFR) Analysis

For single input modulation, equation 12 represents a system with one input (q) and five outputs (C_{CO2}, C_{H2}, C_{CH4}, C_{CO}, C_{H2O}). In order to describe the system behavior, a set of frequency response functions that correlate the dimensionless concentrations (C_i) with the modulated total feed flow rate (q) is derived. We will denote them as H-FRFs ($H_{1,i}(\omega)$, $H_{2,i}(\omega,-\omega)$,…). Nevertheless, when the flow-rate is changing, the mean values of the component concentrations do not fully describe the reactor performance. Instead, it is necessary to consider the component molar flow-rates and their mean values. The dimensionless relative deviations of the molar flow-rates from their steady-state values can be defined in the following way ($i = CO_2$, H_2, CH_4, CO, H_2O):

$$N_i = \frac{F_{tf}(\tau)u_i(\tau) - F_{tf,ss}u_{i,ss}}{F_{tf,ss}u_{i,ss}} \tag{13}$$

In this manuscript, the FRFs which correlate the outlet molar flow rates with the modulated total feed molar flow rate will be denoted as G-FRFs, ($G_{1,i}(\omega)$, $G_{2,i}(\omega,-\omega)$,…). The G

asymmetrical second order FRFs (*G*-ASO FRFs) are derived from the *H*-ASO FRFs. The procedure is described below.

2.2.1 Derivation of the Frequency Response Functions (FRFs)

1. The modulated feed flow rate is defined in the form of cosinusoidal function (A is the modulation amplitude):

$$q(\tau) = A\cos(\omega\tau) = \frac{A}{2}e^{j\omega\tau} + \frac{A}{2}e^{-j\omega\tau} \tag{14}$$

In equation 14 ω is the dimensionless modulation frequency which is defined as follows (ω_d is dimensional frequency in rad/s and SV is the average space velocity in 1/s, i.e., residence time reciprocal):

$$\omega = \frac{\omega_d}{SV_{ss}} \tag{15}$$

2. All outputs (the deviations from the steady state concentrations of all species) are expressed in the Volterra series form:

$$C_i(\tau) = \frac{A}{2}H_{1,i}(\omega)e^{j\omega\tau} + \frac{A}{2}H_{1,i}(-\omega)e^{-j\omega\tau} + \ldots + 2\left(\frac{A}{2}\right)^2 H_{2,i}(\omega,-\omega)e^0 + \ldots \tag{16}$$

3. Equations 15 and 16 are substituted into the set of five equations (for $i = CO_2$, H_2, CH_4, CO, H_2O) described by equation 12.

4. The method of harmonic probing is applied to the equations obtained in step 3, meaning that the terms with the same power of amplitude and frequency (the terms with $(A/2)e^{j\omega\tau}$ corresponding to the first order functions and with $(A/2)^2e^0$ corresponding to the asymmetrical second order function) are collected and equated to zero.

The resulting set of equations for first order FRFs is described as follows:

$$\left(\frac{u_{if,ss}}{u_{i,ss}} - 1\right) = (1+j\omega)H_{1,i}(\omega) + \Lambda_{i,1}H_{1,CH_4}(\omega) + \Lambda_{i,2}H_{1,H_2O}(\omega) + \Lambda_{i,3}H_{1,CO}(\omega) + \Lambda_{i,4}H_{1,CO_2}(\omega) + \Lambda_{i,5}H_{1,H_2}(\omega) \tag{17}$$

The resulting equations for *H*-ASO FRFs are given as follows (Ω_i is given in Appendix B):

$$2\Lambda_{i,1}H_{2,CH_4}(\omega,-\omega) + 2\Lambda_{i,2}H_{2,H_2O}(\omega,-\omega) + 2\Lambda_{i,3}H_{2,CO}(\omega,-\omega) + 2\Lambda_{i,4}H_{2,CO_2}(\omega,-\omega) + 2\Lambda_{i,5}H_{2,H_2}(\omega,-\omega) + 2\Lambda_{i,1}H_{2,i}(\omega,-\omega) = -(1+j\omega)H_{1,i}(\omega) - (1-j\omega)H_{1,i}(-\omega) + \Omega_i \tag{18}$$

5. The equations obtained in step 4 are solved. The set of the first order FRFs described by equation 17 can be written in the matrix form (explicit definitions are given in Appendix C):

$$M_1 \cdot X_1 = N_1 \tag{19}$$

The solution of this equation is

$$X_1 = M_1^{-1} \cdot N_1 \tag{20}$$

Explicit expressions for the first order *H* FRFs can be derived. However, they will not be given here due to their complexity. $H_{1,i}(-\omega)$ is conjugate complex function of $H_{1,i}(\omega)$.[4]

The set of the *H*-ASO FRFs described by equation 18 can be also written in the matrix form (explicit definitions are given in Appendix B):

$$M_2 \cdot X_2 = N_2 \tag{21}$$

The solution is

$$X_2 = M_2^{-1} \cdot N_2 \tag{22}$$

After deriving the *H*-FRFs, the *G*-ASO FRFs can be evaluated as described elsewhere:[6f,h]

$$G_{2,i}(\omega,-\omega) = H_{2,i}(\omega,-\omega) + \frac{1}{2}\left[H_{1,i}(\omega,) + H_{1,i}(\omega)\right] \tag{23}$$

2.2.2 Evaluation of Possible Conversion Increase

As explained previously, for the case when flow rate is modulated, the DC components of the outlet concentrations are not enough for evaluation of possible improvement (increase of CO_2 conversion in this analysis) and the mean outlet molar flow rates should be estimated.[6f,h] The DC component of the dimensionless outlet flow rate of component *i* (equation 13) is defined as follows (superscript *m* refers to a mean, time-averaged value):

$$N_{DC,i} = \frac{\left[F_{tf}(\tau)u_i(\tau)\right]^m - F_{tf,ss}u_{i,ss}}{F_{tf,ss}u_{i,ss}} \tag{24}$$

On the other hand, based on the NFR method, the DC component can be evaluated from the *G*-ASO FRF:

$$N_{DC,i} \approx 2\left(\frac{A}{2}\right)^2 G_{2,i}(\omega,-\omega) \tag{25}$$

Therefore, the mean value of the outlet molar flow rate of a component i can be calculated from the G-ASO FRF as follows:

$$\left(u_i F_{tf}\right)^m \approx u_{i,ss} F_{tf,ss}(1+N_{DC,i}) \tag{26}$$

Finally, the CO_2 conversion for the periodically modulated total feed molar flow rate is defined as follows (superscript m refers to a mean, time-averaged value, $F_{tf,ss}$ is the steady-state value around which the flow rate is modulated):

$$X_{av,CO_2} = \frac{u_{CO_2,f} F_{tf,ss} - \left(u_{CO_2} F_{tf}\right)^m}{u_{CO_2,f} F_{tf,ss}} \tag{27}$$

Combining with equations 25, 26 gives the final form for the CO_2 conversion estimation from the NFR analysis:

$$X_{av,CO_2} \approx 1 - \frac{u_{CO_2,ss}}{u_{CO_2,f}}\left(1+2\left(\frac{A}{2}\right)^2 G_{2,CO_2}(\omega,-\omega)\right) \tag{28}$$

The knowledge of activation energies (E_{aj}) and frequency factors (A_j) is required to calculate kinetic parameters κ_1 and κ_2 (equation 9), which are required in turn to evaluate the FRFs (auxiliary parameters in Appendix B) and, eventually, the CO_2 conversion given by equation 28. Kinetic parameters estimation is described in Appendix D. Another parameter required for the conversion calculation is the Damköhler number corresponding to the chosen steady-state (Da_{ss}, equation 11), as Da_{ss} enters the FRF definitions (auxiliary parameters in Appendix B). For the given pressure (P) and temperature (T), Da_{ss} is inversely proportional to the steady-state space velocity (equation 29, $V_{m,ig}$ is the ideal gas molar volume, ρ_b is the bulk catalyst density).

$$SV_{ss} = \frac{V_{m,ig} F_{tf,ss}}{\rho_b W_c} \tag{29}$$

2.3 The Effect of Periodic Modulation on CO_2 Conversion

2.3.1 Steady State Analysis

As the NFR analysis is applied around a certain average value of the total feed molar flow rate ($F_{tf,ss}$ in equation 11), we first evaluate the steady state CO_2 conversion (X_{CO2}, equation 30) and selectivity to CH_4 formation (S_{CH4}, equation 31) by integrating the set of ODEs described by equation 9 with a constant F_{tf} value, until steady state is achieved (ode15s MATLAB solver, kinetic parameters are given in Appendix D). The resulted steady state conversion and selectivity are plotted as a function of space velocity (equation 29) for different temperatures in Figure 1.

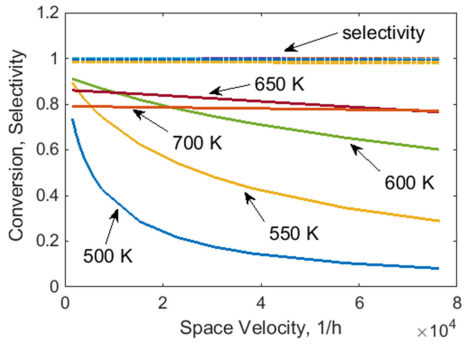

Figure 1. Simulated steady-state CO_2 conversion and CH_4 selectivity as a function of space velocity for different temperatures. Parameters: P = 5 bar, $u_{CO2,f}$ = 0.04, $u_{H2,f}$ = 0.16, $u_{i,f}$ = 0 for i = CH_4, CO, H_2O.

$$X_{CO_2} = \frac{u_{CH_4} + u_{CO}}{u_{CH_4} + u_{CO} + u_{CO_2}} \tag{30}$$

$$S_{CH_4} = \frac{u_{CH_4}}{u_{CH_4} + u_{CO}} \tag{31}$$

As expected for this relatively low temperature range, the selectivity to CH_4 formation is complete in the entire range of space velocities that is no CO formation. Therefore, beyond this point we focus on the CO_2 conversion. Above T = 600 K, the conversion only changes slightly, with a nearly linear decline vs. space velocity, Figure 1. Therefore, periodic modulation of the feed flow rate, that is space velocity modulation, is not expected to affect the CO_2 conversion for T > 600 K. For T = 500-600 K, the conversion decline is nonlinear, thus applying the periodic modulation may result in a nontrivial behavior. We select $SV_{ss} = 7644\ h^{-1}$, which corresponds to $X_{CO2} = 0.43$ at T = 500 K, for further analysis. As it can be seen from Figure 1, for T = 500 K the rate of conversion improvement vs. SV below this point is higher than that above this point (the effect is less pronounced for T = 550, 600 K). Therefore, modulating space velocity around $SV_{ss} = 7640\ h^{-1}$ may result in the overall improvement.

2.3.2 Nonlinear Frequency Response Analysis

In Figure 2, the CO_2 conversion estimated by the NFR method (equation 28) is shown versus the dimensionless modulation frequency for different modulation amplitudes (equations 14, 15). As it can be seen from the results presented in Figure 2, the NFR analysis predicts that the CO_2 conversion will increase in comparison to the steady state value for certain frequencies. The dimensionless modulation frequencies corresponding to the point where the periodic and steady state operation result in identical conversion are ω = 1.38, 4.38, and 15.28 for T = 500, 550, and 600 K, respectively. Below these values, the CO_2 conversion declines as compared to the steady state values. For all cases presented in Figure 2, the deviation from the steady state increases with increasing modulation

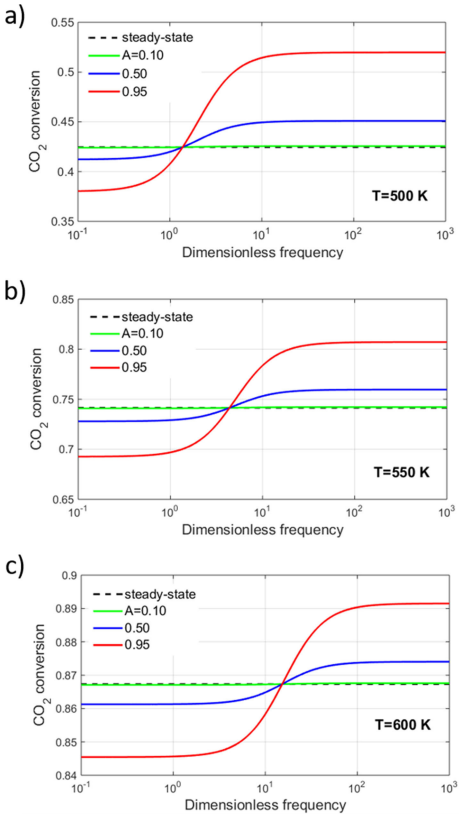

Figure 2. NFR method prediction: CO_2 conversion for periodic operation with flow-rate modulation (equation 28) as a function of the dimensionless forcing frequency for different forcing amplitudes (A = 0.1, 0.5, 0.95) as compared to the corresponding steady state values for T = 500 K (a), 550 K (b), and 600 K (c). Other parameters: P = 5 bar, $SV_{ss} = 7644\ h^{-1}$, $u_{CO2,f} = 0.04$, $u_{H2,f} = 0.16$, $u_{i,f} = 0$ for i = CH_4, CO, H_2O.

amplitude with almost no deviation observed for A = 0.1. The extent of deviation increases with decreasing temperature. For T = 500 K, the NFR analysis predicts that, with the modulation amplitude of A = 0.95, it is possible to improve the CO_2 conversion by 20.8 %. For T = 600 K, the maximal improvement is only 2.6 %.

The increasing conversion enhancement for higher modulation amplitudes and lower temperatures can be attributed to the nonlinear dependence of the CO_2 conversion on space velocity, Figure 1. For T = 500 K, as space velocity is modulated with higher amplitude, the system spends more time at lower space velocities for which the CO_2 conversion is expected to be higher. This enhancement is not fully compensated when the system is shifted to higher space velocities, because the slope of the X_{CO2} vs. SV is lower for $SV > 7600\ h^{-1}$ than for $SV < 4600\ h^{-1}$, Figure 1. For higher temperatures, this effect is less pronounced as it can be seen from Figure 1. Note that according to equation 8, the improvement is proportional to the square of the input amplitude, which provides a mathematical explanation.

Generally speaking, when the feed flow rate (proportional to space velocity) is changed, the system dynamic is playing the main role. The flow rate modulation directly influences the contact (residence) time in the reactor that, in turn, influences the reactant and product concentrations. Owing to the nonlinear reactor dynamics, there could be a phase difference between the flow rate modulation and the concentration changes, and that phase difference changes with the modulation frequency. Conversion enhancement could be achieved if the phase difference assures that when the flow rate is high the reactant concentration is low and vice-versa. In the particular case analyzed herein, this phenomenon takes place at high frequencies. For low frequencies, when the flow rate is high the reactant concentration is also high, and vice-versa, resulting in conversions which are lower than in the steady state operation. The low frequency asymptotes in Figure 2 refer to the time-averaged performance along the cycle. The high frequency asymptote is obtained when that time average does not change with frequency any more.

2.3.3 Numerical Simulations

In order to validate the CO_2 conversion enhancement/deterioration prediction obtained by the NFR analysis, the system of equations described by equation 9 was integrated numerically (ode15s MATLAB solver, kinetic parameters are given in Appendix D) with a modulated total feed flow rate (F_{tf}).

In Figure 3, the transient CO_2 conversion was calculated by equation (30). Note that for no CO formation the CO_2 conversion is equal to the outlet CH_4 molar flow rate normalized by the inlet CO_2 molar flow rate:

$$X_{CO_2} = \frac{u_{CH_4} + u_{CO}}{u_{CH_4} + u_{CO} + u_{CO_2}} \overset{u_{CO}=0}{=} \frac{u_{CH_4} F_t}{(u_{CH_4} + u_{CO_2}) F_t} = \frac{F_{CH_4}}{F_{CH_4} + F_{CO_2}} \equiv \frac{F_{CH_4}}{F_{CO_2,f}} \tag{30a}$$

The numerical simulation results obtained for T = 500 K are shown in time domain, for the modulation frequency of ω = 0.1, with modulation amplitudes of A = 0.5 (a) and 0.95 (b). For A = 0.5 (Figure 3a), the sinusoidal modulation of the feed flow rate (upper panel) results in corresponding nearly sinusoidal fluctuations of concentrations with different amplitudes (middle panel), and transient conversion (bottom panel). As expected, no CO formation was observed.

The resulted overall conversion (equation 27) was very similar to the steady state value obtained with constant feed flow rate (0.41 vs. 0.43). For A = 0.95 (Figure 3b), the system response is nonlinear, with concentration fluctuations significantly deviating from the sinusoidal input. As a result, the obtained transient conversion (equation 30) pattern is also different from the sinusoidal input, with the averaged conversion being actually lower than the corresponding steady state value (0.37 vs. 0.43).

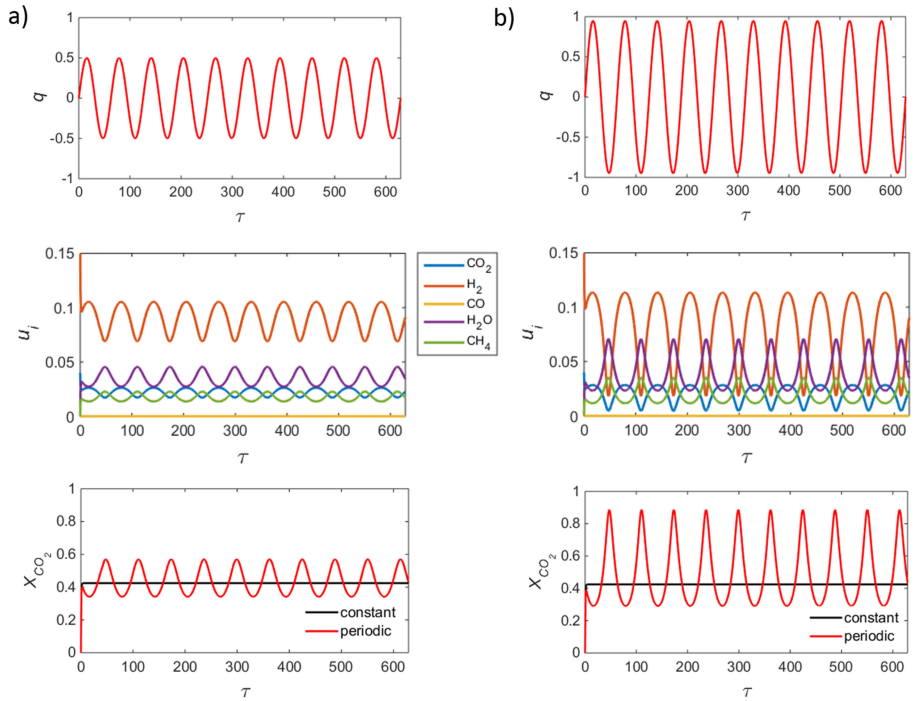

Figure 3. Numerical simulation predictions of the periodic modulation with the modulation frequency $\omega = 0.1$ and amplitude of $A = 0.5$ (a) and $A = 0.95$ (b). The dimensionless total flow- rate modulation (q, upper panels), concentrations (u_i, middle panels), and CO_2 conversions (bottom panels, the unmodulated state is denoted as "constant") are shown. Parameters: T = 500 K, P = 5 bar, $SV_{ss} = 7644\ h^{-1}$, $u_{CO2,f} = 0.04$, $u_{H2,f} = 0.16$, $u_{i,f} = 0$ for i = CH_4, CO, H_2O.

For ω = 10, Figure 4, a small improvement is achieved for A = 0.5 (0.46 vs. 0.43 for constant input), with a substantial conversion enhancement achieved for A = 0.95 (0.63 vs. 0.43), which is in line with the NFR analysis predictions, Figure 2. Similarly to the case with ω = 0.1, the system respond with nearly sinusoidal fluctuations of concentrations for A = 0.5, while the pattern of forced concentration fluctuations for A = 0.95 is shaped differently.

The comparison between the NFR analysis prediction and numerical simulations results is summarized in Table 1, including the case of A = 0.1 as well. In general good agreement was obtained except for the case of ω = 10, A = 0.95, for which the NFR analysis underestimates the conversion enhancement.

Tables 2 and 3 show similar comparison, but for T = 550 K and 600 K and ω = 1, 30 and ω = 1, 100, respectively. Good agreement between the NFR analysis and numerical simulations was achieved (σ shows the percentage deviation of the NFR method prediction from the numerical simulation value).

The results of numerical simulations are summarized in Figure 5, where the overall CO_2 conversion corresponding to the periodic operation (equation 27) is plotted vs. the dimensionless modulation frequency ω (equation 15). While the NFR analysis quantitatively underestimates the deviation from the steady state for high modulation amplitudes, especially for T = 500 K, an excellent agreement is achieved in terms of the prediction of the point where the periodic operation conversion is equal to the steady state value (compare to Figure 2).

Table 1. Comparison between the NFR method prediction and numerical simulation results (denoted as "*num*") for the periodic modulation of flow rate with different modulation amplitudes (A = 0.1, 0.5, 0.95) and modulation frequencies of ω = 0.1, 10. The corresponding steady state conversion is $\mathbf{X_{CO2,ss}} = \mathbf{42.46}$. Parameters: **T = 500 K**, P = 5 bar, $SV_{ss} = 7644\ h^{-1}$, $u_{CO2,f} = 0.04$, $u_{H2,f} = 0.16$, $u_{i,f} = 0$ for i = CH_4, CO, H_2O.

ω	Modulation amplitudes 0.10 X_{CO2} (%)		σ (%)	0.50 X_{CO2} (%)		σ (%)	0.95 X_{CO2} (%)		σ (%)
	num	*NFR*		*num*	*NFR*		*num*	*NFR*	
0.1	42.41	42.41	0	41.21	41.23	0.05	37.12	38.04	2.5
10	42.56	42.56	0	45.46	44.94	-1.1	63.42	51.43	-18.9

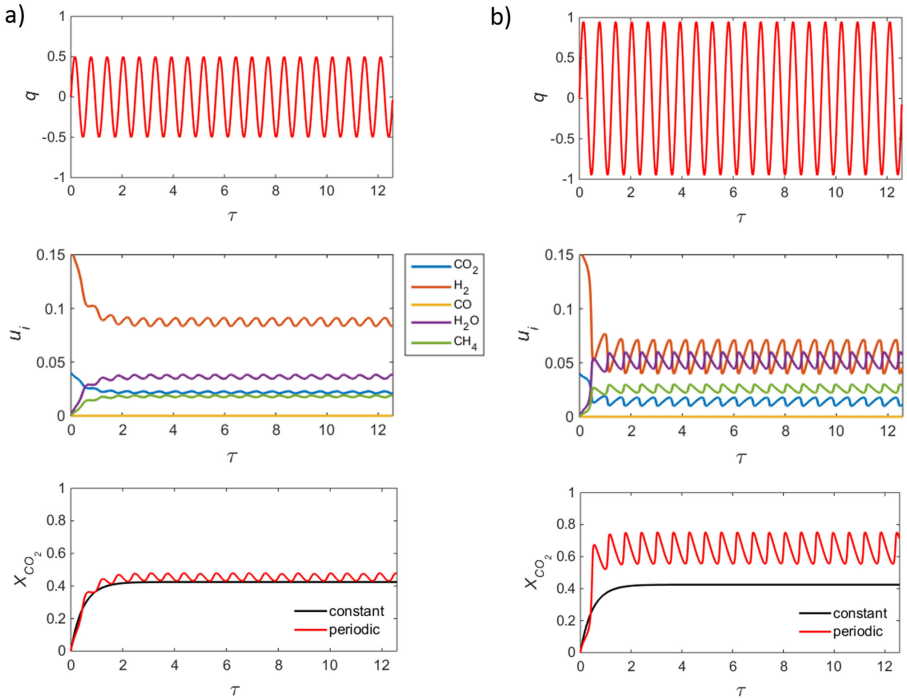

Figure 4. Numerical simulation predictions of the periodic modulation with the modulation frequency $\omega = 10$ and amplitude of $A = 0.5$ (a) and $A = 0.95$ (b). The dimensionless modulation rate (q, upper panels), concentrations (u_i, middle panels), and CO_2 conversions (bottom panels, the unmodulated state is denoted as "constant") are shown. Parameters: T = 500 K, P = 5 bar, $SV_{ss} = 7644\ h^{-1}$, $u_{CO2,f} = 0.04$, $u_{H2,f} = 0.16$, $u_{i,f} = 0$ for i = CH_4, CO, H_2O.

Table 2. Comparison between the NFR method prediction and numerical simulation results (denoted as "*num*") for the periodic modulation of flow rate with different modulation amplitudes (A = 0.1, 0.5, 0.95) and modulation frequencies of ω = 0.1, 10. The corresponding steady state conversion is $X_{CO2,ss} = 74.14$. Parameters: **T = 550 K**, P = 5 bar, $SV_{ss} = 7644\ h^{-1}$, $u_{CO2,f} = 0.04$, $u_{H2,f} = 0.16$, $u_{i,f} = 0$ for i = CH_4, CO, H_2O.

	Modulation amplitude								
	0.10			0.50			0.95		
ω	X_{CO2} (%)		σ (%)	X_{CO2} (%)		σ (%)	X_{CO2} (%)		σ (%)
	num	NFR		num	NFR				
1	74.11	74.10	-0.01	73.24	72.91	-0.45	70.57	69.69	-1.25
30	74.22	74.21	-0.01	76.14	75.88	-0.34	86.30	80.40	-6.84

Table 3. Comparison between the NFR method prediction and numerical simulation results (denoted as "*num*") for the periodic modulation of flow rate with different modulation amplitudes (A = 0.1, 0.5, 0.95) and modulation frequencies of ω = 0.1, 10. The corresponding steady state conversion is $X_{CO2,ss} = 86.73$. Parameters: **T = 600 K**, P = 5 bar, $SV_{ss} = 7644\ h^{-1}$, $u_{CO2,f} = 0.04$, $u_{H2,f} = 0.16$, $u_{i,f} = 0$ for i = CH_4, CO, H_2O.

	Forcing amplitude								
	0.10			0.50			0.95		
ω	X_{CO2} (%)		σ (%)	X_{CO2} (%)		σ (%)	X_{CO2} (%)		σ (%)
	num	NFR		num	NFR		num	NFR	
1	86.71	86.71	0	86.14	86.13	-0.01	84.61	84.56	-0.06
100	86.76	86.76	0	87.45	87.37	-0.09	90.25	89.03	-1.35

As it was shown above, the NFR analysis can be used to predict the conversion enhancement or deterioration as a result of the periodic modulation of the feed flow rate, as it was validated by numerical simulations to this point (experimental validation is still required). Good agreement is obtained in terms of the conversion deviation from its steady state value upon periodic forcing. Excellent agreement was achieved between the NFR method analysis and predictions obtained by numerical simulation in terms of identifying the point where the periodic operation conversion is equal to the steady state

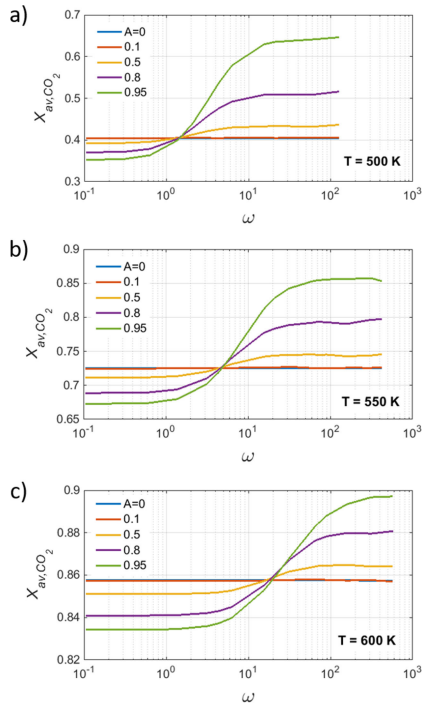

Figure 5. Numerical simulations prediction of the conversion corresponding to periodic modulation of the total flow-rate plotted vs dimensionless frequency for different modulation amplitudes of A = 0 (steady-state), 0.1, 0.5, 0.8, 0.95. Parameters: P = 5 bar, SV_{ss} = 7644 h^{-1}, $u_{CO2,f}$ = 0.04, $u_{H2,f}$ = 0.16, $u_{i,f}$ = 0 for i = CH_4, CO, H_2O; T = 500 K (a), 550 K (b), 600 K (c).

value in frequency domain (ω = 1.38, 4.38, and 15.28 for T = 500, 550, and 600 K, respectively).

In all cases analyzed, for frequencies lower than the point where the periodic operation conversion is equal to the steady state value, conversion declines achieving a plateau. For higher frequencies, conversion increases attaining a maximum value as well, Figures 2, 5. The inflection point location is clearly correlated with the temperature, being shifted to higher frequencies for higher temperature. This finding indicates that a certain correlation between the modulation frequency and reaction rate is required to achieve conversion enhancement; further investigation is required to clarify this phenomenon.

For practical applications, it is important to analyze the system in dimensional time domain, because certain (high) frequencies may not be realistic to achieve in a real setup. Dimensional frequency is calculated from equation (15) for a given space velocity (SV_{ss} = 7644 h^{-1} corresponds to a residence time of 0.47 s). The dimensional period is calculated from the ω_d value converted to Hz (1 rad/s is 1/2π Hz), i.e., ω = 10 corresponds to the modulation period of 0.3 s (for SV_{ss} = 7644 h^{-1}).

Therefore, periodic modulation for ω > 10 is not suitable for practical implementation as it is impossible to modulate the inlet flow rate with such short modulation periods. Thus the CO_2 conversion enhancement for T = 550 K and T = 600 K would not be practically achievable (Figure 5). On the other hand, for T = 500 K a very substantial conversion improvement is possible for frequencies as low as ω = 5 at large modulation amplitudes.

Numerical simulation results obtained for T = 500 K with ω = 5 (modulation period 0.6 s), A = 0.95 and ω = 5 (modulation period 0.3 s), A = 0.99 are shown in Figures 6 and 7 respectively. The CO_2 conversion enhancement is substantial for both cases, being 30.2 % and 62.8 % correspondingly. In both cases, the system response to periodic modulation is highly nonlinear, with concentrations fluctuating in distinct patterns completely different from the shape of the forced sinusoidal modulation of the feed flow rate. It is interesting that reactants (H_2 and CO_2) and products (CH_4 and H_2O) respond with different patterns (middle panels in Figures 6, 7). It will be very intriguing to observe such patterns in an experimental setup, which is a subject of the near future work.

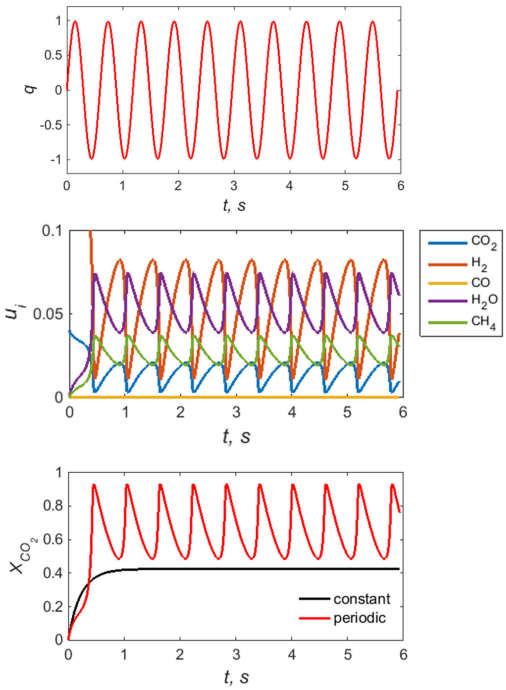

Figure 6. Numerical simulation predictions of the periodic modulation with the modulation frequency **ω = 5** and amplitude **A = 0.95**. The dimensionless modulation rate (q, upper panel), concentrations (u_i, middle panel), and CO_2 conversion (bottom panel, the unmodulated state is denoted as "constant") are shown. The average conversion is $X_{av,CO2}$ = 0.56 (vs. 0.43 for constant input). Parameters: T = 500 K, P = 5 bar, SV_{ss} = 7644 h^{-1}, $u_{CO2,f}$ = 0.04, $u_{H2,f}$ = 0.16, $u_{i,f}$ = 0 for i = CH_4, CO, H_2O.

3. Conclusions

We have demonstrated that the Nonlinear Frequency Response (NFR) method can be implemented to forecast the CO_2 conversion enhancement in a periodically operated Sabatier

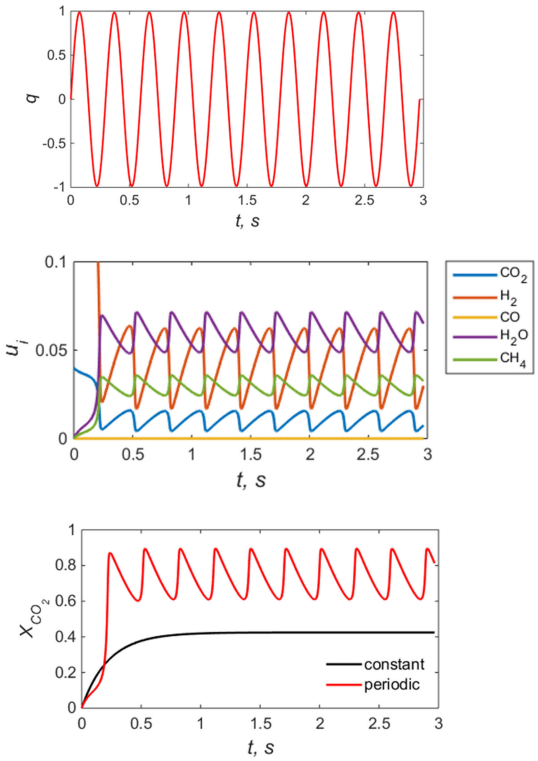

Figure 7. Numerical simulation prediction of the periodic modulation with the modulation frequency $\omega = 10$ and amplitude $A = 0.99$. The dimensionless modulation rate (q, upper panel), concentrations (u_i, middle panel), and CO_2 conversion (bottom panels, the unmodulated state is denoted as "constant") are shown. The average conversion is $X_{av,CO2} = 0.70$ (vs. 0.43 for constant input).Parameters: T = 500 K, P = 5 bar, $SV_{ss} = 7644\ h^{-1}$, $u_{CO2,f} = 0.04$, $u_{H2,f} = 0.16$, $u_{i,f} = 0$ for i = CH_4, CO, H_2O.

reactor converting CO_2 into synthetic CH_4. Periodic forcing was assumed to be applied through a sinusoidal modulation of the feed flow rate in the low temperature regime (T = 500–600 K) in which the CO_2 conversion is kinetically limited. The analytical predications obtained by the NFR analysis using experimentally determined kinetic parameters for the Ni/α-Al_2O_3 catalyst and a flow reactor model were validated versus numerical simulations, with a good agreement achieved.

The NFR analysis, based on the derivation of frequency response functions (FRFs), predicted a significant conversion gain of up to 50 % for certain modulation frequencies above the point where the periodic operation conversion is equal to the steady state value in the plot of CO_2 conversion vs. modulation frequency. The conversion enhancement is higher for high modulation frequencies, with that point being shifted to higher frequencies at higher temperatures. A clear relationship between this point location and operating temperature indicates that a certain degree of correlation between the modulation frequency and reaction rate is required for conversion improvement.

Both the NFR analysis and numerical simulations predict that it is possible to obtain 70 % CO_2 conversion at 500 K, 5 bar, and average space velocity of 7,600 h^{-1} by a periodic modulation of the feed flow rate, as compared to the corresponding steady state CO_2 conversion of 43 %. The obtained results are intriguing with a high potential for practical application subject to experimental confirmation. Altogether, the abovementioned findings are of great importance for advancing the field of the thermocatalytic CO_2 conversion in general and for the CO_2 conversion via the Sabatier reaction in particular.

Nomenclature

A	dimensionless modulation frequency, equation 14
A_j	frequency factor of the rate coefficient of reaction j, units of k_j
c_i	molar concentration of species i, mol/m^3
C_i	dimensionless deviation from the steady state concertation, equation 12
Da	Damköhler number, equation 9
E_{aj}	activation energy of reaction j, kJ/mol
$G_{2,i}$	second order G-type frequency response function
f_j	dimensionless reaction rate, equation 10
F_i	molar flow rate of species i, mol/s
F_t	total molar flow rate, mol/s
$H_{1,i}$	first order G-type frequency response function
$H_{2,i}$	second order H-type frequency response function
k_j	rate constant of reaction j, (mol bar^2)/(kg s) for $j = 1, 3$; mol/(kg s bar) for $j = 2$
$k_{j,eq}$	dimensionless equilibrium constant, equation 10
$K_{j,eq}$	equilibrium constant of reaction j, bar^2 ($j = 1, 3$); dimensionless ($j = 2$)
L	catalyst bed length, m
N_i	dimensionless flow rate of species i, equation 23
$N_{i,DC}$	DC component of the dimensionless flow rate of species i, equation 24
p_i	partial pressure of species i, bar
P	pressure, bar
q	dimensionless modulation rate, equation 12
R_j	rate of reaction j, mol/(kg s)
R_g	gas constant, kJ/(mol K)
S_{CH_4}	selectivity to CH_4 formation, equation 31
SV	space velocity, h^{-1} (s^{-1}), equation 29
t	time, s
T	temperature, K
u_i	dimensionless concentration of species i, equation 9
v_g	gas velocity, m/s
$V_{m,ig}$	ideal gas molar volume, m^3/mol
W_c	catalyst weight, kg
X_{CO_2}	CO_2 conversion, equation 30
X_{av,CO_2}	time-averaged CO_2 conversion, equations 27, 28

Greek letters

α_{ij} stoichiometric coefficient of species i in reaction j
δ outlet-to-inlet molar density ratio
κ_j dimensionless reaction rate, equation 9
ρ_b bulk catalyst density, kg/m^3
τ dimensionless time, equation 9
ω dimensionless modulation frequency, equation 15

Subscripts

f feed
ss steady state (constant input)
t total

Superscripts

m mean (average) value

Appendix

A. Dimensional Reaction Rates

The original dimensional reaction terms were adopted from the literature (for simplicity, it is assumed that $den = 1$; $K_{j,eq}$ is equilibrium constant):[2c,8]

$$R_1 = \frac{k_1}{p_{H_2}^{2.5}}\left(p_{CH_4}p_{H_2O} - \frac{p_{H_2}^3 p_{CO}}{K_{1,eq}}\right)\frac{1}{den^2}$$

$$R_2 = \frac{k_2}{p_{H_2}}\left(p_{CO}p_{H_2O} - \frac{p_{H_2}p_{CO_2}}{K_{2,eq}}\right)\frac{1}{den^2}$$

$$R_3 = \frac{k_3}{p_{H_2}^{3.5}}\left(p_{CH_4}p_{H_2O}^2 - \frac{p_{H_2}^4 p_{CO_2}}{K_{3,eq}}\right)\frac{1}{den^2}$$

$$k_j = A_j \exp\left(\frac{-E_j}{R_g T}\right)$$

Although these rate expression were originally derived for the CH_4 steam reforming (MSR) reaction system,[8] they predict well the Sabatier-RWGS reaction system[2b,c] (the reverse system of MSR).

B. Expansion of Nonlinear Kinetic Terms

The nonlinear kinetic terms f_1, f_2 and f_3 (equation 10) are first written in terms of deviations from steady state values (C_i) and then expanded in the Taylor series around the steady-state point (only the first and second order terms are shown).

(i) Expansion of Nonlinear Term f_1

The kinetic term f_1 written as a function of C_i is given as follows:

$$f_1 = S_1\frac{(C_{CH_4}+1)(C_{H_2O}+1)}{(C_{H_2}+1)^{2.5}} + S_2(C_{H_2}+1)^{0.5}(C_{CO}+1)$$

Expansion of f_1 in Taylor series around the steady-state ($C_{is}=0$):

$$f_1 = f_1^{ss} + f_1^d$$

$$f_1^{ss} = S_1 + S_2$$

$$f_1^d = S_1C_{CH4} + S_1C_{H2O} + [-2.5S_1 + S_2]C_{H2} + \frac{2.5\times 3.5}{2}S_1C_{H2}^2 + S_2C_{CO} + S_1C_{CH4}C_{H2O} + [-2.5]S_1C_{CH4}C_{H2} + [-2.5]S_1C_{H2O}C_{H2} + S_2C_{H2}C_{CO} +$$

(ii) Expansion of Nonlinear Term f_2

The kinetic term f_2 written as a function of C_i is given as follows:

$$f_2 = P_1\frac{(C_{CO}+1)(C_{H2O})}{(C_{H2}+1)} + P_2(C_{CO2}+1)$$

$$P_1 = \delta\frac{u_{CO,s}u_{H2O,s}}{u_{H2,s}} \qquad P_2 = -\delta\frac{u_{CO2,s}}{k_{2eq}}$$

Expansion of f_2 in Taylor series around the steady-state ($C_{is}=0$):

$$f_2 = f_2^{ss} + f_2^d$$

$$f_2^{ss} = P_1 + P_2$$

$$f_2^d = P_1C_{CO} + P_1C_{H2O} - P_1C_{H2} + P_1C_{H2}^2 + P_2C_{CO2} + P_1C_{CO}C_{H2O} - P_1C_{CO}C_{H2} - P_1C_{H2O}C_{H2} +$$

(iii) Expansion of Nonlinear Term f_3

The kinetic term f_3 written as a function of C_i is given as follows:

$$f_3 = R_1\frac{(C_{CH_4}+1)(C_{H_2O}+1)^2}{(C_{H_2}+1)^{3.5}} + R_2(C_{H_2}+1)^{0.5}(C_{CO2}+1)$$

$$R_1 = \frac{1}{\sqrt{\delta}} \frac{u_{CH4,s} u_{H2O,s}{}^2}{u_{H2,s}^{3.5}} \qquad R_2 = -\delta^{1.5} \frac{u_{H2,s}^{0.5} u_{CO2,s}}{k_{3eq}}$$

Expansion of f_3 in Taylor series around the steady-state ($C_{is}=0$):

$$f_3 = f_3^{ss} + f_3^d$$

$$f_3^{ss} = R_1 + R_2$$

$$f_3^d = R_1 C_{CH4} + 2R_1 C_{H2O} + R_1 C_{H2O}^2 + [-3.5R_1 + 0.5R_2] C_{H2} + \left[\frac{3.5 \times 4.5 R_1 - 0.5^2 R_2}{2}\right] C_{H2}^2 + R_2 C_{CO2} + 2R_1 C_{CH4} C_{H2O} + [-3.5] R_1 C_{CH4} C_{H2} + [-3.5 \times 2] R_1 C_{H2O} C_{H2} + 0.5 R_2 C_{H2} C_{CO2} +$$

Finally, the expansion of all non-linear terms is given with the following equation:

$$\frac{Da}{u_{i,s}} \left(\alpha_{i1}\kappa_1 f_1^d + \alpha_{i2}\kappa_2 f_2^{bd} + \alpha_{i3} f_3^d\right) = (-\Lambda_{i,1} C_{CH4} - \Lambda_{i,2} C_{H2O} - \Lambda_{i,3} C_{CO} - \Lambda_{i,4} C_{CO2} - \Lambda_{i,5} C_{H2} + W_{i,1} C_{H2O}^2 + W_{i,2} C_{H2}^2 + W_{i,3} C_{CH4} C_{H2O} + W_{i,4} C_{CH4} C_{H2} + W_{i,5} C_{H2O} C_{CO} + W_{i,6} C_{H2O} C_{H2} + W_{i,7} C_{H2} C_{CO} + W_{i,8} C_{H2} C_{CO2})$$

The auxiliary parameters are defined in the following way:

$$\Lambda_{i,1} = -\frac{Da_{ss}}{u_{i,s}} [\alpha_{i1}\kappa_1 S_1 + \alpha_{i3} R_1]$$

$$\Lambda_{i,2} = -\frac{Da_{ss}}{u_{i,s}} [\alpha_{i1}\kappa_1 S_1 + \alpha_{i2}\kappa_2 P_1 + 2\alpha_{i3} R_1]$$

$$\Lambda_{i,3} = -\frac{Da_{ss}}{u_{i,s}} [\alpha_{i1}\kappa_1 S_2 + \alpha_{i2}\kappa_2 P_1]$$

$$\Lambda_{i,4} = -\frac{Da_{ss}}{u_{i,s}} [\alpha_{i2}\kappa_2 P_2 + \alpha_{i3} R_2]$$

$$\Lambda_{i,5} = -\frac{Da_{ss}}{u_{i,s}} [\alpha_{i1}\kappa_1(-2.5S_1 + S_2) + \alpha_{i2}\kappa_2(-P_1) + \alpha_{i3}(-3.5R_1 + 0.5R_2)]$$

$$W_{i,1} = \frac{Da_{ss}}{u_{i,s}} [\alpha_{i3} R_1]$$

$$W_{i,2} = \frac{Da_{ss}}{u_{i,s}} \left[\alpha_{i1}\kappa_1 \left(\frac{2.5 \times 3.5}{2} S_1\right) + \alpha_{i2}\kappa_2 (P_1) + \alpha_{i3} \left(\frac{3.5 \times 4.5 R_1 - 0.5^2 R_2}{2}\right)\right]$$

$$W_{i,3} = \frac{Da_{ss}}{u_{i,s}} [\alpha_{i1}\kappa_1 S_1 + 2\alpha_{i3} R_1]$$

$$W_{i,4} = \frac{Da_{ss}}{u_{i,s}} [\alpha_{i1}\kappa_1(-2.5S_1) + \alpha_{i3}(-3.5R_1)]$$

$$W_{i,5} = \frac{Da_{ss}}{u_{i,s}} [\alpha_{i2}\kappa_2 P_1]$$

$$W_{i,6} = \frac{Da_{ss}}{u_{i,s}} [\alpha_{i1}\kappa_1(-2.5S_1) + \alpha_{i2}\kappa_2(-P_1) + \alpha_{i3}(-3.5^*2) R_1]$$

$$W_{i,7} = \frac{Da_{ss}}{u_{i,s}} [\alpha_{i1}\kappa_1 S_2 + \alpha_{i2}\kappa_2(-P_1)]$$

$$W_{i,8} = \frac{Da_{ss}}{u_{i,s}} [\alpha_{i3} 0.5 R_2]$$

C. Derivation of the Frequency Response Functions (FRFs)

In ***step 4***, Ω_i is given as follows:

$$\begin{aligned}\Omega_i = {} & (2W_{i,1} H_{1,H2O}(\omega) H_{1,H2O}(-\omega) + 2W_{i,2} H_{1,H2}(\omega) H_{1,H2}(-\omega) \\ & + W_{i,3}\left(H_{1,CH4}(\omega) H_{1,H2O}(-\omega) + H_{1,CH4}(-\omega) H_{1,H2O}(\omega)\right) \\ & + W_{i,4}\left(H_{1,CH4}(\omega) H_{1,H2}(-\omega) + H_{1,CH4}(-\omega) H_{1,H2}(\omega)\right) \\ & + W_{i,5}\left(H_{1,H2O}(\omega) H_{1,CO}(-\omega) + H_{1,H2O}(-\omega) H_{1,CO}(\omega)\right) \\ & + W_{i,6}\left(H_{1,H2O}(\omega) H_{1,H2}(-\omega) + H_{1,H2O}(-\omega) H_{1,H2}(\omega)\right) \\ & + W_{i,7}\left(H_{1,H2}(\omega) H_{1,CO}(-\omega) + H_{1,H2}(-\omega) H_{1,CO}(\omega)\right) \\ & + W_{i,8}\left(H_{1,H2}(\omega) H_{1,CO2}(-\omega) + H_{1,H2}(-\omega) H_{1,CO2}(\omega)\right))\end{aligned}$$

In ***step 5***, M_1, X_1, N_1 are given as follows:

$$M_1 = \begin{pmatrix} (\Lambda_{CH4,1} + 1 + j\omega) & \Lambda_{CH4,2} & \\ \Lambda_{H2O,1} & (\Lambda_{H2O,2} + 1 + j\omega) & \\ \Lambda_{CO,1} & \Lambda_{CO,2} & \\ \Lambda_{CO2,1} & \Lambda_{CO2,2} & \\ \Lambda_{H2,1} & \Lambda_{H2,2} & \\ \Lambda_{CH4,3} & \Lambda_{CH4,4} & \Lambda_{CH4,5} \\ \Lambda_{H2O,3} & \Lambda_{H2O,4} & \Lambda_{H2O,5} \\ (\Lambda_{CO,3} + 1 + j\omega) & \Lambda_{CO,4} & \Lambda_{CO,5} \\ \Lambda_{CO2,3} & (\Lambda_{CO2,4} + 1 + j\omega) & \Lambda_{CO2,5} \\ \Lambda_{H2,3} & \Lambda_{H2,4} & (\Lambda_{H2,5} + 1 + j\omega) \end{pmatrix}$$

$$X_1 = \begin{pmatrix} H_{1,CH4}(\omega) \\ H_{1,H2O}(\omega) \\ H_{1,CO}(\omega) \\ H_{1,CO2}(\omega) \\ H_{1,H2}(\omega) \end{pmatrix} \quad N_1 = \begin{pmatrix} \left(\frac{u_{CH4,f,s}}{u_{CH4,s}} - 1\right) \\ \left(\frac{u_{H2O,f,s}}{u_{H2O,s}} - 1\right) \\ \left(\frac{u_{CO,f,s}}{u_{CO,s}} - 1\right) \\ \left(\frac{u_{CO2,f,s}}{u_{CO2,s}} - 1\right) \\ \left(\frac{u_{H2,f,s}}{u_{H2,s}} - 1\right) \end{pmatrix}$$

In ***step 5***, M_2, X_2, N_2 are given as follows:

$$M_2 = \begin{pmatrix} 2(1+\Lambda_{CH4,1}) & 2\Lambda_{CH4,2} & 2\Lambda_{CH4,3} & 2\Lambda_{CH4,4} & 2\Lambda_{CH4,5} \\ 2\Lambda_{H2O,1} & 2(\Lambda_{H2O,2}+1) & 2\Lambda_{H2O,3} & 2\Lambda_{H2O,4} & 2\Lambda_{H2O,5} \\ 2\Lambda_{CO,1} & 2\Lambda_{CO,2} & 2(\Lambda_{CO,3}+1) & 2\Lambda_{CO,4} & 2\Lambda_{CO,5} \\ 2\Lambda_{CO2,1} & 2\Lambda_{CO2,2} & 2\Lambda_{CO2,3} & (\Lambda_{CO2,4}+1) & 2\Lambda_{CO2,5} \\ 2\Lambda_{H2,1} & 2\Lambda_{H2,2} & 2\Lambda_{H2,3} & 2\Lambda_{H2,4} & 2(\Lambda_{H2,5}+1) \end{pmatrix}$$

$$X_2 = \begin{pmatrix} H_{2,CH4}(\omega,-\omega) \\ H_{2,H2O}(\omega,-\omega) \\ H_{2,CO}(\omega,-\omega) \\ H_{2,CO2}(\omega,-\omega) \\ H_{2,H2}(\omega,-\omega) \end{pmatrix}$$

$$N_2 = \begin{pmatrix} -(1+j\omega)H_{1,CH4}(\omega) - (1-j\omega)H_{1,CH4}(-\omega) + \Omega_{CH4} \\ -(1+j\omega)H_{1,H2O}(\omega) - (1-j\omega)H_{1,H2O}(-\omega) + \Omega_{H2O} \\ -(1+j\omega)H_{1,CO}(\omega) - (1-j\omega)H_{1,CO}(-\omega) + \Omega_{CO} \\ -(1+j\omega)H_{1,CO2}(\omega) - (1-j\omega)H_{1,CO2}(-\omega) + \Omega_{CO2} \\ -(1+j\omega)H_{1,H2}(\omega) - (1-j\omega)H_{1,H2}(-\omega) + \Omega_{H2} \end{pmatrix}$$

D. Kinetic Parameters Estimation

In order to estimate E_{aj} and k_j values (total 6 parameters), a set of experiments was performed using a flow system similar to that described elsewhere[7] and a commercial reforming Ni/α-Al_2O_3 catalyst (12 wt% Ni, BASF, supplied by Research Catalysts, Inc. USA). A typical result of the activation energy evaluation is shown in Figure 8. Briefly, CO_2 and H_2 are fed by mass flow controllers to a lab scale flow reactor containing ~0.5 g of the catalyst with the outlet concentrations continuously monitored using an infrared analyzer.[7]

CO_2 conversion and selectivity to CH_4 formation are evaluated by equations 30, 31. For the activation energy evaluation, tests are performed under differential conditions, i.e., conversion less than 20 %, which is a standard laboratory technique in heterogeneous catalysis studies.[7] The obtained activation energies did not differ significantly from the originally reported values,[8] and the E_{a1}, E_{a2}, E_{a3} values from the literature were adopted (240, 67, and 244 kJ/mol respectively).

In order to obtain the frequency factors, another set of experiments were conducted varying both temperature and space velocity. Next, the numerical solution obtained by integrating a set of ODEs described by equation 9 (MATALB ode15 s) was fitted to experimental data using least squares analysis. The results are shown in Figure 9. The obtained frequency factors were 3.6E+16 and 8.86E+15 (mol bar$^{0.5}$)/

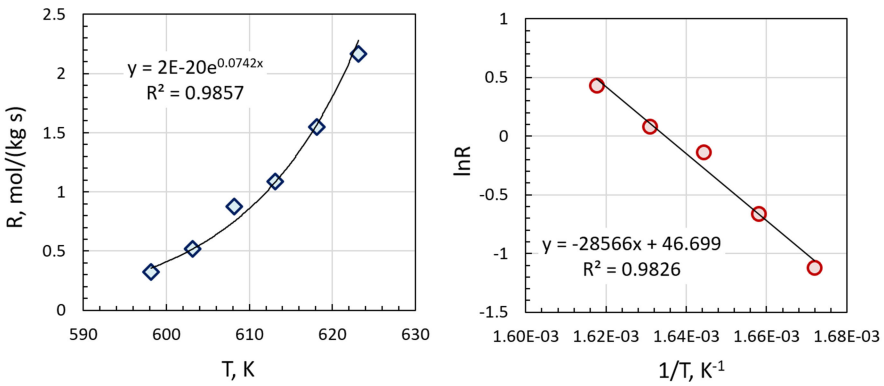

Figure 8. A typical activation energy evaluation experiment, showing the CO_2 conversion rate (R) vs. temperature and the corresponding logarithmic plot (the activation energy is evaluated from the slope of the lnR vs. 1/T plot). Experimental conditions: $H_2/CO_2 = 2$ in the feed, 2.5 L/min total flow, 300 mg of catalyst (Ni/a-Al_2O_3 diluted 4-fold with g-Al_2O_3), P = 3 bar.

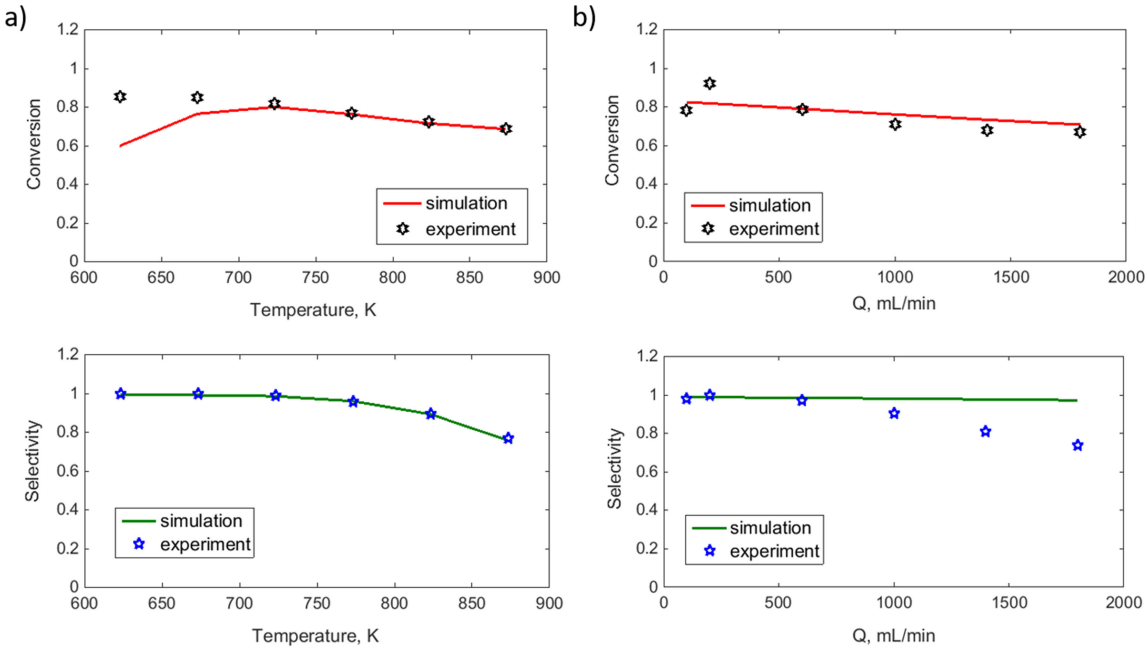

Figure 9. Simulation results vs. experimental data in terms of conversion and selectivity as a function of temperature (a) and feed flow rate (b). Experimental conditions: $H_2/CO_2 = 4$ in the feed, P = 3 bar, 300 mg of undiluted Ni/a-Al_2O_3 catalyst, 450 mL/min total flow (a) and T = 723 K (b).

(g h) for A_1, A_3 and 1.35E+7 mol/(g bar h) for A_2 (approximately 7–9 times higher than those in the original publication[8]). Although the model overestimates conversion at low temperature and fail to predict selectivity decline at elevated space velocities, in general good agreement was obtained for the purpose of the initial NFR method analysis demonstration.

Acknowledgements

The authors acknowledge funding support from the Natural Science and Engineering Research Council (NSERC) of Canada through the NSERC Discovery Grant program. Part of this research was also supported by the Ministry of Education, Science and Technological Development of the Republic of Serbia, through research projects ON172022 and III45001.

References

[1] a) W. Wang, S. Wang, X. Ma, J. Gong, *Chem. Soc. Rev.* **2011**, *40*, 3703–3727; b) M. D. Porosoff, B. Yan, J. G. Chen, *Energy Environ. Sci.* **2016**, *9*, 62–73.

[2] a) D. S. A. Simakov, *Renewable Synthetic Fuels and Chemicals from Carbon Dioxide*, Springer International Publishing, **2017**; b) D. Sun, F. M. Khan, D. S. A. Simakov, *Chem. Eng. J.* **2017**, *329*, 165–177; c) D. Sun, D. S. A. Simakov, *J. CO_2 Util.* **2017**, *21*, 368–382; d) T. Schaaf, J. Grünig, M. R. Schuster, T. Rothenfluh, A. Orth, *Energ. Sustain. Soc.* **2014**, *4*, 2.

[3] L. Xua, H. Yang, M. Chen, F. Wang, D. Nie, L. Qi, X. Lian, H. Chen, M. Wu, *J. CO_2 Util.* **2017**, *21*, 200–210.

[4] M. Petkovska, A. Seidel-Morgenstern, in *Periodic Operation of Reactors* (Eds.: P. L. Silveston, R. R. Hudgins), Elsevier, Amsterdam, **2013**, pp. 387–413.

[5] a) J. M. Douglas, *Process Dynamics and Control*, Prentice-Hall, Englewood Cliffs, New Jersey, **1972**; b) D. D. Weiner, J. F. Spina, *Sinusoidal Analysis and Modeling of Weakly Nonlinear Circuits*, Van Nostrand Reinhold Company, New York, **1980**.

[6] a) A. Markovic, A. Seidel-Morgenstern, M. Petkovska, *Chem. Eng. Res. Des.* **2008**, *86*, 682–691; b) D. Nikolić-Paunić, M. Petkovska, *Chem. Eng. Sci.* **2013**, *104*, 208–219; c) D. Nikolić, A. Seidel-Morgenstern, M. Petkovska, *Chem. Eng. Sci.* **2014**, *117*, 71–84; d) D. Nikolić, A. Seidel-Morgenstern, M. Petkovska, *Chem. Eng. Sci.* **2014**, *117*, 31–44; e) D. Nikolić, A. Seidel-Morgenstern, M. Petkovska, *Chem. Eng. Sci.* **2015**, *137*, 40–58; f) D. Nikolić, M. Felischak, A. Seidel-Morgenstern, M. Petkovska, *Chem. Eng. Tech.* **2016**, *39*, 2126–2134; g) D. Nikolić, M. Petkovska, *Chemie Ing. Technik* **2016**, *88*, 1715–1722; h) D. Nikolić, A. Seidel-Morgenstern, M. Petkovska, *Chem. Eng. Tech.* **2016**, *39*, 2020–2028.

[7] D. S. A. Simakov, H. Y. Luo, Y. Román-Leshkov, *Appl. Catal. B: Environ.* **2015**, *168–169*, 540–549.

[8] J. Xu, G. F. Froment, *AIChE J.* **1989**, *35*, 88–96.

Received: December 1, 2017
Accepted: February 7, 2018
Published online on February 27, 2018